Vortex-slip transitions in superconducting *a*-NbGe mesoscopic channels

N. Kokubo,* T. G. Sorop,† R. Besseling,‡ and P. H. Kes
Kamerlingh Onnes Laboratory, Leiden University, P.O. Box 9504, 2300 RA, Leiden, The Netherlands
(Received 27 February 2006; revised manuscript received 3 May 2006; published 16 June 2006)

Intriguing and novel physical aspects related to the vortex flow dynamics have been recently observed in mesoscopic channel devices of *a*-NbGe with NbN channel edges. In this work we have systematically studied the flow properties of vortices confined in such mesoscopic channels as a function of the magnetic field history, using dc-transport and mode-locking (ML) measurements. As opposed to the field-down situation, in the field-up case a kink anomaly in the dc *I-V* curves is detected. The mode-locking measurements reveal that this anomaly is, in fact, a flow induced vortex slip transition: by increasing the external drive (either dc or ac) a sudden change occurs from n to $n+2$ moving vortex rows in the channel. The observed features can be explained in terms of an interplay between field focusing due to screening currents and a change in the predominant pinning mechanism.

DOI: 10.1103/PhysRevB.73.224514 PACS number(s): 74.25.Qt, 74.78.Na, 74.25.Fy, 83.50.Ha

I. INTRODUCTION

Vortex matter in type II superconductors is an ideal system for studying the motion of periodic media in pinning environments. In recent years, we concentrated our investigations on the properties of confined vortex matter in weak pinning mesoscopic channels, which were nanofabricated in double layers of amorphous (*a*-)NbGe (weakly pinned) and NbN (strongly pinned) thin films.[1,2] Other studies of vortex flow through channels bounded by pinned vortices have been performed in several experimental configurations, e.g., Josephson vortices at low-angle grain boundaries in high-T_c superconductors moving through pinned Abrikosov vortices.[3,4] Moreover, easy flow channels for Abrikosov vortices were artificially fabricated by using antidot arrays[5,6] or by laser processing.[7] Our system offers the possibility to study the flow properties systematically for both plastic and defective vortex configurations, while continuously tuning the vortex lattice structure inside the channels by changing the applied magnetic field. Novel physical aspects related to the commensurability have been recently observed in such channel devices.[8,9] These include unusual oscillations of critical current and flow resistance with magnetic field.[2] The relationship between those oscillations and the commensurability has been elucidated by mode-locking (ML) experiments.[2,10,11] Furthermore, using the ML technique important information about vortex flow has been obtained and it was possible to detect the dynamic ordering/melting transition predicted by Koshelev and Vinokur.[12]

So far our studies were carried out in field-down (FD) or field-cooled (FC) conditions. Under these conditions the screening currents along the channel walls are weak and do not play a significant role. However, in the field-up (FU) case these screening currents cannot be ignored giving rise to interesting magnetic field history effects. In this work we explore the consequences of such effects on the dynamics of the confined vortices. It turns out that the screening currents generate a particular vortex configuration and field distribution around the channel which can be characterized by field focusing. This effect is especially strong at the lowest fields. A consequence of this distinct configuration is an entirely different behavior of the flow dynamics compared to that in the field-down case. Using dc-transport, mode-locking, and flux flow resistivity measurements we performed a systematic study of the vortex dynamics for increasing fields. We observe a change from weak intrinsic pinning to strong shear interaction determining the pinning mechanism and the dynamic properties. We find compelling evidence for a flow induced vortex slip transition between the vortex rows inside the same channel and also a crossover from one dimensional (1D) to two dimensional (2D) in the vortex flow behavior. The 2D vortex flow is the Bardeen-Stephen type of flow, in which the flux-flow resistance has a linear dependence in H, whereas the 1D is characterized by a $\sqrt{H}$ dependence. This issue is quite relevant in the view of recent works on confined low dimensional flow, for instance, the depinning of a classic quasi-one-dimensional Wigner crystal.[13]

The paper is structured as follows. In Sec. II a few details are given about the samples fabrication and geometry, as well as the experimental techniques used. In Sec. III the results of the measurements are presented followed by an extensive discussion. The critical current data are used to propose a simple physical model based on the field focusing effect. Then the model is substantiated by mode-locking and flux flow resistivity experiments. Finally, in Sec. IV the conclusions are presented.

II. EXPERIMENTAL DETAILS

The samples used in this study consist of easy flow vortex channels (see the inset of Fig. 1). They are fabricated using a similar recipe to the one used in Ref. 1. First double layers consisting of weak pinning (*a*-)$Nb_{1-x}Ge_x$ film (thickness $d=550$ nm and $x\approx 0.3$) and strong pinning NbN film ($d=50$ nm) are rf-sputtered successively without breaking the vacuum. Then reactive ion etching, with proper masking, was used to remove the top layer and to make deep trenches down to the middle of the bottom layer.[1] As a result, the (remaining) NbGe layer in the channels is $d_{ch}\approx 300$ nm thick. Identical straight channels (300 in parallel), with lengths of 300 μm, and at 10 μm spacing were fabricated. Applying magnetic field perpendicular to the films induces

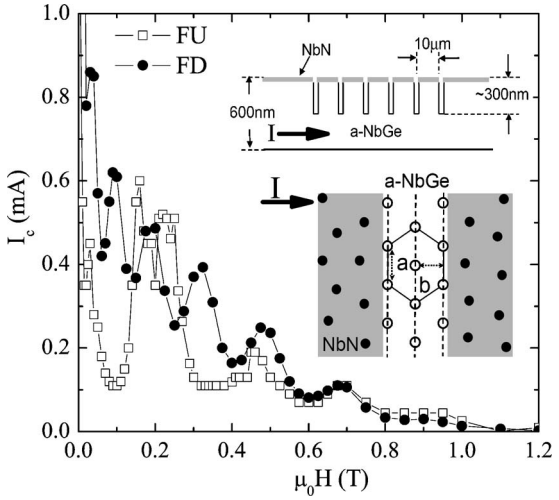

FIG. 1. Comparison between the critical current I_c measured in FU and FD at 1.9 K. Both data show commensurate-incommensurate oscillations but below 0.5 T they behave differently. The insets show schematic drawings of the channel sample: cross-section perpendicular to channels and top-view indicating the vortex structure in the channels and channel edges. The drawings are not on scale. The arrows show the direction of the applied current.

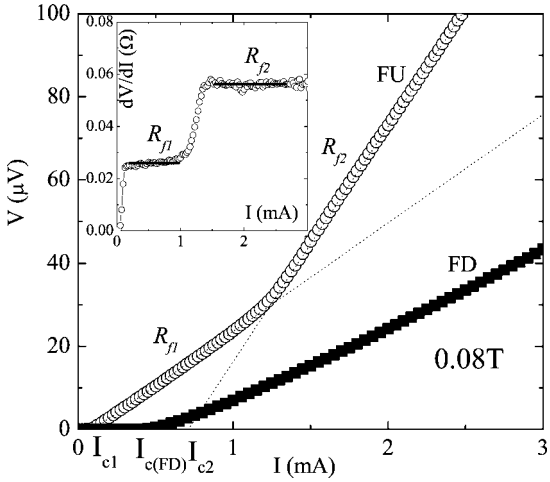

FIG. 2. dc *I-V* curves at $T=1.9$ K and $\mu_0 H=0.08$ T for FU and FD cases. For the FU curve the two mobility regimes are characterized by two different critical currents, I_{c1} and I_{c2}, defined from the linear extrapolations (the dashed lines). The inset shows the calculated differential resistance $R_d=dV/dI$ vs current for the FU case.

vortices (see inset of Fig. 1). Outside the channels vortices are strongly pinned by the NbN layer, whereas the ones situated inside the channel experience both the bulk (intrinsic) pinning from NbGe and the shear interaction with the strongly pinned edge vortices. When a transport current is applied perpendicular to the channels it will drive the channel vortices along the channels while those from the banks remain pinned creating easy flow vortex channels.

dc-transport and ML experiments were performed on samples with different channel widths. We focus here on the experimental results obtained in a device with $w=230$ nm channel width. All measurements were done in a four-point contact geometry with samples immersed in (superfluid) ^{4}He in order to prevent heating. In the case of ML experiments the rf-current leads were attached to the dc-current leads very close to the sample and the results were obtained by measuring the dc voltage. The current as well as the voltage pads are made on top of the NbN layer (for more details see Refs. 1 and 2).

Before performing any measurement, we first cooled the sample in zero field (ZFC) to 1.9 K (well below $T_{c,NbGe} \approx 2.68$ K or $T_{c,NbN} \approx 11$ K). In the FU procedure the field was increased at a very slow sweep rate ($\leqslant 1$ mT/s) to the target value. The results were compared to those obtained in the FD procedure which was performed by first applying a field higher than $\mu_0 H_{c2}=1.6$ T of NbGe and then ramping it down to the target value.

III. RESULTS AND DISCUSSIONS

A. Critical currents

A plot of the critical current (I_c) versus field (H) is given in Fig. 1 for both the FU and FD procedures. I_c is obtained from the dc *I-V* measurements and is defined using a constant 1 μV criterion. As observed in the figure, in both cases the critical currents show an oscillatory behavior. The FD data have been already explained in detail in a previous paper[2] as a sequence of commensurate-incommensurate transitions. The pinning potential for vortices inside the channels is dominated by the shear interaction with the strongly pinned vortices in the channel edges. By varying the external field H one can continuously tune the commensurability between the row spacing (b_0) and the channel width and thus change the defect structure and number of confined rows. ML experiments have shown[2,11] that, contrary to the previous interpretations, I_c is maximized at mismatch while minima appear at matching. Numerical simulations have demonstrated jamming of driven vortices occurring at mismatch and elucidated the important role of disorder arrangements of the pinned vortices in the channel edges for the flow dynamics.[2,9]

In Fig. 1 one can see that, while above 0.6 T the FU and FD data coincide, below 0.6 T they are clearly different. In order to study in more detail this difference we first analyze the *I-V* characteristics in both FU and FD cases. Typical results for $\mu_0 H < 0.15$ T are shown in Fig. 2 ($\mu_0 H = 0.08$ T). While for currents above $I_{c,FD}$, the FD curve exhibits the expected linear behavior, the FU curve first shows a linear region up to ≈ 1.3 mA and, then at a kink there is a sudden change to another linear branch with higher slope. The differential resistance (dV/dI vs I) plot shown in the inset clearly demonstrates this anomaly: two plateaus of differential resistance with a steplike increase at the "kink." These two mobility regions: low mobility (below the kink) and high mobility (above the kink) can be characterized by two different critical currents, I_{c1} and I_{c2}, defined by extrapolating the linear fits (dashed lines in Fig. 2) until they intersect the x axis. Clearly $I_{c1} < I_{c,FD} < I_{c2}$.We mention here that the measured *I-V* curves are reversible with respect to the sweep in current and that the value and the field dependence

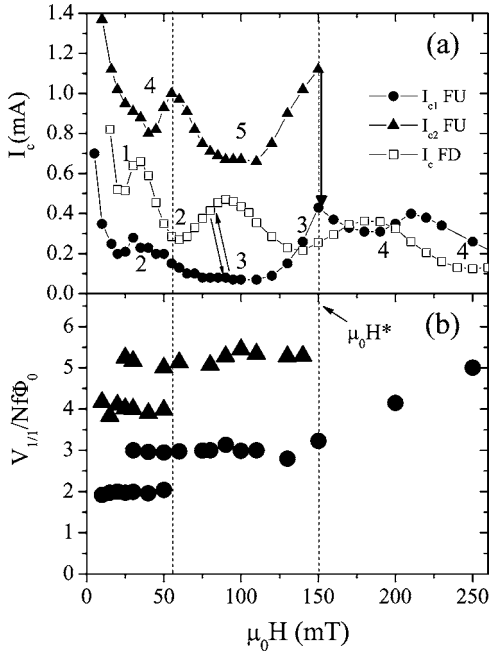

FIG. 3. (a) History dependent behavior of the critical current at small fields $H<H^*$: I_{c1} is small and oscillates smoothly, whereas I_{c2} shows similar commensurate oscillations as $I_{c,FD}$. (b) The number of coherently moving rows is determined from ML experiments over ≈200 channels for the FU case [they are also indicated on the plots around the minima in (a) in order to compare to the FD case].

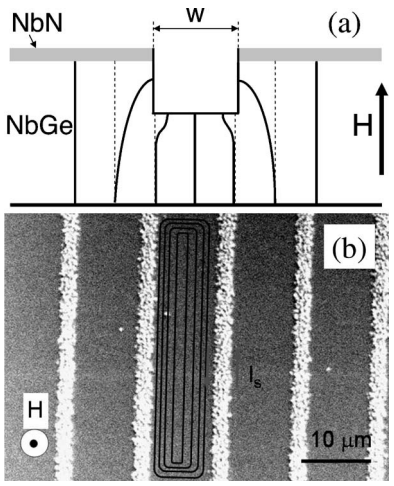

FIG. 4. (a) Schematic illustration of the flux line configuration around a channel in increasing and decreasing fields. The thick lines (FU case) are bent down from the straight broken lines (FD case) due to the field focusing effect of the screening currents along the channel edges; (b) scanning electron microscopy (SEM) picture after magnetic decoration of a sample with $w=1.5$ μm (at 0.05 T, FU). The screening currents flowing in the NbN islands are also indicated.

of I_{c1} are very similar to the critical current as defined by the 1 μV criterion.

Let us now focus our attention on the field dependence of these critical currents. Figure 3(a) displays their small field (<0.25 T) behavior. As discussed above, $I_{c,FD}$ shows commensurability oscillations. The number of coherently moving rows, as determined from ML experiments,[2] is indicated in the figure at the minima (matching condition). In the FU case I_{c1} and I_{c2} show different behaviors. Apart from a small peak at ≈30 mT, I_{c1} decreases monotonously when increasing H, and then stays nearly constant up to ≈120 mT where it increases rapidly. This dependence is clearly different from the oscillations observed in the FD case. Moreover, the magnitude of I_{c1} is very small. Expressed in terms of pinning force density we obtain $F_p \approx 1\times 10^5$ N/m^3 for $\mu_0 H \approx 0.08$ T. This is significantly smaller than the shearing force density (typically $3-6\times 10^5$ N/m^3), but much closer to the bulk pinning F_p in the a-NbGe layer alone, for which we estimate a value of $\approx 0.5\times 10^5$ N/m^3 at $H=0.05H_{c2}$ and $T=0.7T_c$.[14] In contrast to I_{c1}, I_{c2} is considerably bigger and exhibits large oscillations, similar to the FD case but with maxima and minima at different H values. Increasing the field above 0.12 T produces an increase in the nonlinearity of the I-V curve around the kink which becomes gradually less well defined. Above $\mu_0 H^* \approx 0.15$ T the kink in the I-V curves disappears and, therefore, one can only speak about I_{c1}. Its magnitude is now of the same order as $I_{c,FD}$ and, although not in phase, it has a similar oscillatory behavior.

From the magnitude and the character of the oscillations of the critical currents we conclude that, below H^*, I_{c1} is determined by the bulk pinning of the a-NbGe layer, whereas I_{c2} is mainly due to the shear interaction with the vortices in the channel edges (CE). On the other hand, above H^* the critical current is dominated by the shear interaction with the static vortices in the CE, just as in the FD case. In fact, the difference between the FU and the FD cases becomes smaller and smaller and at around 0.6 T it vanishes completely (see Fig. 1). The reversible switch between the FU and the FD branches, illustrated with double arrow at $\mu_0 H \approx 70-90$ mT, will be discussed in the next section.

In order to explain the features observed for increasing field we sketch in Fig. 4(a) a possible field profile around a channel. Let us consider the situation when there are three vortex rows confined in the channels. Since for these values of thickness and fields the a-NbGe is described by the 2D collective pinning theory[14] (the longitudinal Larkin length $L_c \gg d_{ch}$), one expects that everywhere in the sample the flux lines will be straight (broken lines in the figure), if the effect of the screening currents along the channel edges can be ignored. This situation corresponds, in fact, to the FD case where the screening currents are so small that they may be neglected. However, the situation is different in the FU case, where the flux first penetrates into the NbGe layer of the channels and only at higher fields into the NbN layer and the CE ($H_{p,NbN} > H_{p,NbGe}$, where H_p is the field of first flux penetration[9,15]). Due to screening currents along the channel walls and in the top layer, the outer two flux lines [thick lines in Fig. 4(a)] are expelled from the NbN layer and bend away from their original positions (broken lines), resulting in a possible termination of those flux lines at the channel walls and in a field focussing effect above the channel. The first (strongly) pinned vortices in the NbN layer are located far away from the channel walls. As a result, at least for small fields, the shear potential induced on the outer two rows inside the channel is large, while it is very small for the inner

rows, since the shear potential decays exponentially towards the middle of the channel.[9]

The field-focusing effect above the channels was directly confirmed by decoration experiments.[9] Figure 4(b) shows a SEM image of a channel device with $w=1.5$ μm decorated at $\mu_0 H=0.05$ T, in FU. During decoration, Ni particles are driven to the channels by field gradients induced by the screening currents flowing along the CE and as a result a strong concentration of them is seen in and around the channels. Note that the absence of Ni clusters in the NbN layer results from the "capture" of the Ni particles by strong field gradients and does not mean that in the inner NbN layer the field is zero. The paths and directions of the screening currents running in CE are also drawn in the figure.

Based on this model about the field profile in the channels, we can now explain the dc *I-V* curves as follows. At small currents ($I_{c1}<I<I_{c2}$) only the three inner (weakly pinned) rows are moving. When increasing the current above the kink value ($I>I_{c2}$) the outer two rows are depinned and start moving as well. Consequently, we can state that the kink represents a flow induced *dynamic* transition between n and $n+2$ moving vortex rows. Moreover, the small value of I_{c1}, i.e., it is of the order of the intrinsic critical current of *a*-NbGe, can be explained by assuming the presence of misfit dislocations. These dislocations will have Burger vectors parallel to the channels and lie between outer and inner rows.[9] The nonmoving outer rows will screen the disorder present in CE from the inner rows and, therefore, the inner rows will only feel the intrinsic *a*-NbGe pinning.

B. Mode-locking experiments

In order to check the validity of this model and to further elucidate the nature of the vortex slip transition we have performed ML experiments on our samples. ML is a dynamic resonance between an ac drive—superimposed on the dc drive—and the dynamic lattice modes excited collectively (by the dc drive) at the "washboard" ($q=1$) and higher ($q\geq 2$) frequencies $f_{int}=qv/a$,[16–18] where v and a are the average velocity and the distance between the vortices in the channel, and q an integer number. It has already been proven[2,10,11] that ML is an excellent tool to explore the vortex flow configuration in the channels. For $pf=f_{int}$ interference steps appear in the *I-V* curves at $V_{p/q}=(p/q)f\Phi_0 n$, where Φ_0 is the flux quantum, n the number of moving vortex rows per channel, and p and q integers.

Figure 5 shows the dc *I-V* curves taken in the FU case with and without a superimposed ac drive at $f=30$ MHz in 0.08 T ($<\mu_0 H^*$). Clear ML steps appear at equidistant voltage levels ($p/q=1/1$, 2/1, and 3/1) corresponding to the fundamental and the two higher harmonics. For this value of the frequency the steps occur in the high-mobility branch and correspond to a coherent motion of $n=5$ rows. Upon reducing f, the voltage for each ML step decreases linearly down to about 10 MHz. Below this frequency, the fundamental ML step appears in the low-mobility branch and it persists down to at least 1 MHz. Such a ML step, occurring in the low mobility branch, can clearly be seen as a peak in a plot of the differential conductance (dI/dV vs V) at 6 MHz in the inset of Fig. 5.

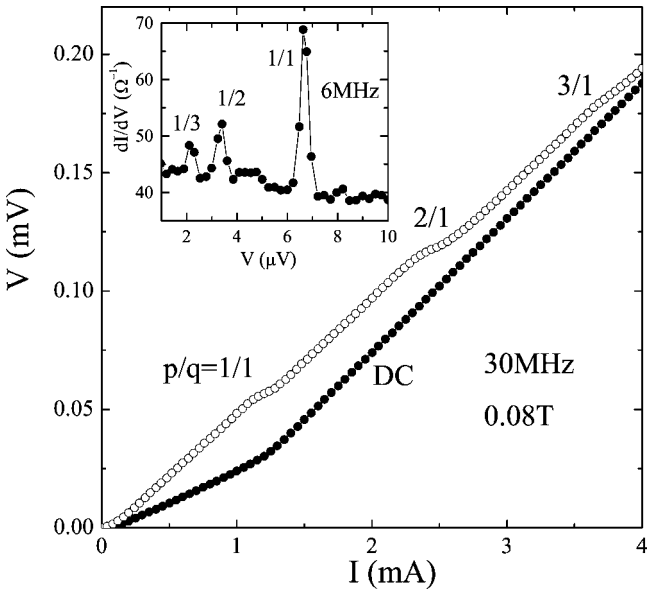

FIG. 5. dc *I-V* curves measured at 0.08 T in the FU case with and without a superimposed 30 MHz ac current. ML interference steps are observed for the fundamental voltage [$(p/q=1/1)$ and harmonics (2/1, 3/1)] in the high-mobility branch. The inset shows dI/dV vs V in the low-mobility regime measured when a 6 MHz ac current is superimposed. Subharmonic ML peaks at $p/q=1/3$, 1/2 as well as the fundamental peak (1/1) are observed.

To obtain further insight in this transition, we have performed systematic measurements at different magnetic fields varying both the frequency and the amplitude of the superimposed rf signal. We note that varying the rf-frequency f corresponds to probing the coherently moving vortex lattice at different dc velocities via the (fundamental) ML condition $f=v/a$. In order to directly compare with the dc *I-V* curves we plot, for $\mu_0 H=0.08$ T in Fig. 6(a), $V_{1/1}$ as a function of the dc-drive I, instead of f. To illustrate the variation of the number of coherently moving rows we further divide $V_{1/1}$ by f, Φ_0 and the number of active channels $N=180$.[19] Two plateaus of $V_{1/1}/\Phi_0 f$ appear at high and low dc drives, respectively, in good agreement with the two resistive plateaus in R_d shown in the inset of Fig. 2. By taking into account that $V_{1/1}$ is measured over $\approx 200(=N_{ch})$ parallel channels, it becomes clear that at low mobility three rows are coherently moving in the channels while at the kink voltage a dynamic change and a transition to five moving rows occur. Note that compared to the dc *I-V* curves the value of the current corresponding to the kink is slightly lower, which is to be expected since the superimposed rf drive shifts downwards both the kink as well as the depinning currents (see, for instance, Fig. 5).

In Fig. 6(b) we display the change of the width of ML current step. This is a very useful tool since it shows to what extent the n vortex rows move coherently, i.e., it probes the average coherent fraction per channel.[10] ΔI_{max} is defined as the maximum width of the ML step with respect to the rf amplitude, for fixed frequency and field. Upon approaching the dynamic transition by increasing f and, therefore, probing higher dc-currents, ΔI_{max} in the $n=3$ regime decreases and seems to vanish around 0.7 mA, while ΔI_{max} for $n=5$

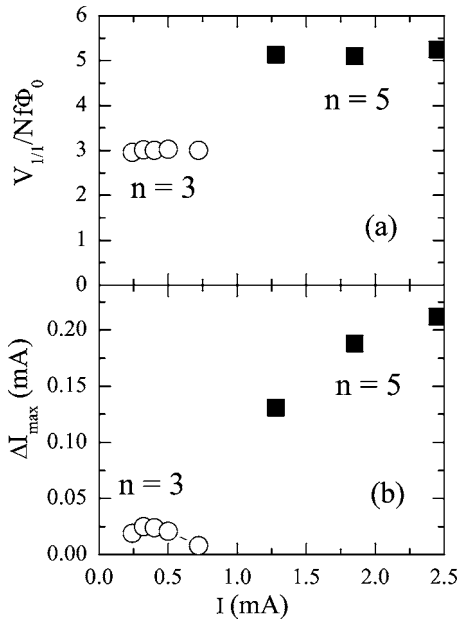

FIG. 6. The dependence of (a) the fundamental ML voltage and (b) the width of ML current step on the dc-drive at $\mu_0 H = 0.08$ T in the FU case.

appears around 1 mA and grows monotonously with the current. This behavior implies that the dynamic change upon increasing the dc drive consists of a continuous reduction of the coherently moving fraction of three rows and a subsequent growth of the coherently moving fraction of five rows. We, thus, conclude that the ML data confirm the dc *I-V* data and the assumptions and the model discussed above.

In contrast to what is probed when f is varied, an increase in the rf-amplitude (I_{rf}) probes the ac-induced vortex slip transition. In Fig. 7 we plot the dependence of the normalized $V_{1/1}$ on I_{rf}. At small rf amplitudes ($I_{rf} < 1$ mA) we have a plateau which corresponds to $n=3$ rows moving coherently in the channels. At large ac drive ($I_{rf} > 2$ mA) $V_{1/1}$ is constant as well, corresponding to $n=5$ moving rows, proving that we deal here with an ac-induced transition from n to $n+2$ rows. Between 1 and 2 mA we find that the differential conductance peaks corresponding to the ML effect (ML peaks) are very broad and quite difficult to assign to a precise number of coherently moving rows in the channels. This anomaly, which has been observed around the transition in all our measurements, can be explained if we consider in detail the mechanism related to the unpinning of the extra two rows. Since the outer two rows feel the effect of the shear interaction with the static vortices situated well inside the NbN strip, when starting to move they will also experience a different (higher) friction force than the inner rows. As a consequence, just after transition, their velocities will be smaller than the velocities of the inner rows giving rise to a (concave) velocity profile. This makes the ML peaks rather broad and not very well defined. However, an increase in the ac drive has the effect of healing the differences in friction and, in a similar way as the dynamic friction is smaller than the static friction in classical mechanics, the outer two rows will experience less and less friction at higher rf amplitudes. This effect will gradually suppress the differences in velocities and for $I_{rf} > 1.5$ mA the ML peaks become well defined and their voltage values correspond to the expected value for $n+2=5$ rows.

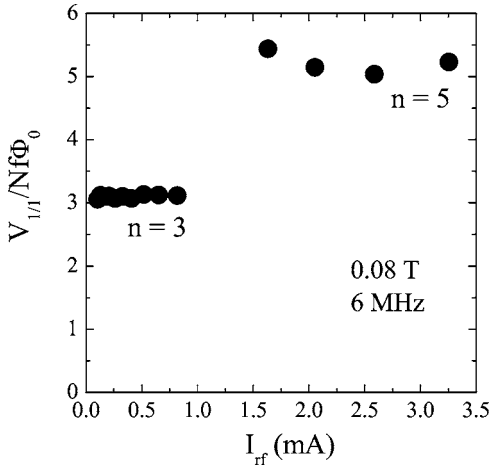

FIG. 7. ac-driven vortex slip transition at $\mu_0 H = 0.08$ T and for $f=6$ MHz. Increasing I_{rf} a jump from $n=3$ to $n=5$ occurs. Just above the transition $V_{1/1}$ shows an anomalous dependence on the rf amplitude.

Qualitatively the same features observed for three (five) vortex rows are seen for $\mu_0 H < 50$ mT where the transition takes place from $n=2$ to $n=4$. Therefore, we summarize in Fig. 3(b) the dependence of the (normalized) fundamental ML voltage $V_{1/1}/N\Phi_0 f$ on the magnetic field for $H < H^*$. Let's first focus on the low field behavior of the number of rows. In the high mobility branch (triangles) the flow structure displays a four-row configuration for $\mu_0 H < 50$ mT, while a five-row configuration emerges for $\mu_0 H > 30$ mT. Thus, multiple flow configurations of four and five rows occur around 50 mT, indicating a mismatch condition. This is in fact in good agreement with the peak observed in I_{c2} in Fig. 3(a) at $\simeq 0.05$ T. In the low mobility branch (circles) a similar field evolution of flow configurations from two to three rows is observed. However, the peak in I_{c1} appears at $\simeq 30$ mT and is less pronounced. This is not very surprising since in the low mobility regime the inner rows are screened from the edge disorder and feel both the intrinsic potential and the shear interactions which leads to a suppression of the oscillatory behavior. Moreover, we briefly mention here that the sharptransition plotted in Fig. 2 for $\mu_0 H = 0.08$ T is not typical. Depending on the matching conditions and, therefore, on the field, we find that the sharp change from a linear low-mobility to a linear high-mobility branch is replaced by either positive or negative curvatures of *I-V* curves around the kink. This behavior is caused by the, above mentioned, delicate interplay between the intrinsic pinning and the edge disorder.[9] A more detailed study would be required to come to a complete description.

At higher fields, close to H^*, both I_{c1} and I_{c2} show a steep increase related to the onset of the incommensurate peak. However, as already mentioned in the previous section, we detect in the *I-V* curves a gradual disappearance of the kink and the appearance of a nonlinear behavior and, for $H > H^*$, one can no longer define a second critical current or two

distinct mobility regions. The effect is accompanied by a gradual loss of coherency as detected in the ML experiments. Increasing the field above 0.12 T leads to smaller and smaller ML steps ($\Delta I < 1$ μA) and eventually vanishing of the ML effect for $0.15 < \mu_0 H < 0.2$ T. The fact that I_{c1} has now a value that is on the same order as $I_{c,FD}$ can be understood by a reduction in the influence of screening currents and straightening of the outer flux lines. Although the difference in FD and FU seems almost entirely suppressed, their "out-of-phase" oscillations point towards a slightly increased flux density in the channels in the FU case. That is confirmed by ML measurements which detects at $\mu_0 H = 0.2$ T a higher number of rows, $n=4$, compared to $n=3$ detected in the FD case.

1. Reversible transitions

Another interesting feature related to the field history effects is the behavior of the system when the direction of varying the field is changed. We observe that when the field is decreased anywhere in the FU branch (for $H < H^*$), the critical current $I_{c,1}$ switches to the FD branch. See, for instance, indicated with an arrow in Fig. 3(a), the transition from 90 to 70 mT. For small sweep rates ($dB/dt < 1$ mT/s), as in the experiments presented here, the response is also reversible upon a subsequent field increase: $I_{c,FD}$ returns to the FU branch. A similar switching behavior has been previously reported[1] and interpreted as switching between different lattice orientations. We give here a different explanation for this effect based on findings in detailed mode-locking measurements performed at intermediate fields between 90 and 70 mT sweeping the field in both directions. What we found is that indeed not only the critical current but also the vortex configurations and the number of moving rows switch reversibly. That can be explained by the change of the outer vortex lines from a bent shape (FU case) to a straight line (FD case) and back to the bent shape, which is possible for small sweep rates.

2. Subharmonic steps

As is seen in the inset of Fig. 5 we detected subharmonic peaks in the low mobility branch, i.e., in the regime in which only the inner rows are mobile and in which the (de)pinning is mainly determined by the intrinsic pinning of the NbGe. This is quite remarkable because the previous attempts to detect subharmonics in the FD and the FC case (for which the pinning is dominated by the shear interaction with channel edges) have failed. It has been previously shown[14] that the pinning centers in our amorphous NbGe thin films are density fluctuations with length scales of the order ξ ($\leqslant 10$ nm), distributed randomly. Since these scales are much smaller than the average vortex spacing for the field of interest ($a_0 \geqslant 50$ nm), the intrinsic pinning can excite lattice modes at harmonics of the washboard frequency qv/a, with $q \geqslant 1$.[16,20] Therefore, the coupling between the external rf drive and the dynamic lattice modes will result in subharmonics steps, as observed here. In fact our findings are in good agreement with the old experiments of Fiory[20] and the recent results of Kokubo *et al.*[21] in which subharmonics were found in weakly pinning films of Al, and single crystals of $NbSe_2$, respectively.

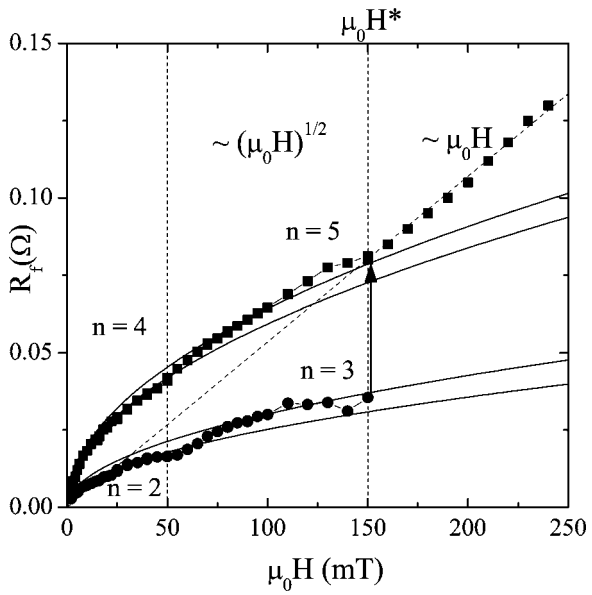

FIG. 8. Field dependence of the flux-flow resistance (R_f) at small fields $H < 0.25$ T, as determined from the dc *I-V* curves. The experimental data (circles for low mobility, and squares for high mobility) are shown together with their best fits of $\propto \sqrt{H}$ for $H < H^*$ and linear dependence H for $H > H^*$. Around 50 mT jumps in R_f occur due to the change in the number of moving rows from n to $n+1$.

C. Flux-flow resistance

We finally turn to the relation between the flux-flow resistance and the vortex flow configurations. The field dependence of the flux flow resistance (R_f) is shown in Fig. 8 for $\mu_0 H < 0.25$ T. R_f is determined from the linear fit of the *I-V* curves in both low-mobility and high-mobility regions. For $\mu_0 H < 50$ mT we see that in the low mobility regime (two moving vortex rows; circles) as well as in the high mobility branch (four rows; squares), R_f increases as $\sqrt{H}$. The small jumplike increase in both branches at about 50 mT marks the increase from n to $n+1$ moving vortex rows. Up to H^* the data still follow a $\sqrt{H}$ dependence. In fact, a double logarithmic plot of the $R_f(H)$ data shows $R_f \propto H^\alpha$ behavior with $\alpha = 0.5 \pm 0.03$ in all cases. Finally, at $H = H^*$ the $\sqrt{H}$ behavior disappears and a $R_f \propto H$ dependence is observed. This linear dependence is the usual 2D flux flow behavior (see below) whereas the $\sqrt{H}$ behavior is expected for 1D flux flow. Such 1D behavior has been observed in case of motion of a single vortex chain along a low-angle grain boundary in high-T_c superconductors.[3]

Numerical simulations for our channel system[9] have shown that quasi-1D behavior occurs for weak disorder potentials. In this case the mobility is governed by the glide of edge dislocations along the channel or the nucleation of stacking faults of interstitials and vacancies.[9] We think that this weak disorder description is appropriate here for the low field FU experiments, because the screening currents of the

CE suppresses the effect of the strong positional disorder of the vortices in the NbN layer. The transverse degrees of freedom for the displacements of the channel vortices is thereby strongly suppressed, leading to a quasi-1D behavior sustained by (misfit) dislocations with sideplanes oriented along the channels.

We can quantitatively estimate the flux flow resistance if we consider the general formula

$$R_f = \rho_f \frac{w_{dyn} N_{ch}}{l d_{ch}}, \tag{1}$$

where d_{ch} is the thickness of the NbGe film in the channels, N_{ch} is the total number of channels, and w_{dyn} is the dynamic width of the channel (measuring the drop of the voltage over the channel) which depends on the number of moving rows. ρ_f is the flux flow resistivity as computed by Larkin and Ovchinnikov.[22,23]

If we consider that the effective width of the channel $w_{dyn}=nb$ is field dependent (b is the spacing between the rows moving in the channels) and substitute it in Eq. (1) we obtain

$$R_f \propto \sqrt{H}. \tag{2}$$

Using for the normal state resistance of the a-NbGe film $\rho_n = 2.2 \times 10^{-6}\ \Omega$ m, we can estimate the magnitude of the flux density $B_{ch}/\mu_0 H$ enhancement in the channels. Obviously $B_{ch}/\mu_0 H$ depends on the magnitude of the screening currents and is expected to decrease with the increase of H. For $\mu_0 H < 0.05$ T we find values as high as $B/\mu_0 H \approx 6.5$ and 3.7, for the high-mobility and low-mobility branches. Above 0.05 T, $B_{ch}/\mu_0 H$ is smaller starting from 1.9 in the high-mobility branch and 1.1 in the low-mobility branch implying that the field focusing is weakened (as expected with increasing the field).

Above $\mu_0 H^*$, where the screening currents are small, the transverse degrees of freedom in inner and outer rows become equally important and all the vortices in the channel become fully coupled. The strong disorder present (in the CE which is not screened anymore) leads to plasticity inside the channel and one, therefore, expects that the vortex flow recovers the (conventional) 2D nature observed in the FD case. Indeed we see in Fig. 8 that R_f becomes linear in field

$$R_f \propto H. \tag{3}$$

Thus, we can state that H^* is a cross-over field which marks a change from a quasi-1D to a conventional 2D flux flow.

Finally, we mention that careful analysis of the flux-flow resistance data provides also interesting information about the density of the vortex lattice inside the channels. If we consider the ratio of flow resistances in the high-mobility branch to that in the low-mobility branch $r = R_{f,H}/R_{f,L}$ and we follow its dependence on field we see that for $\mu_0 H < 0.05$ T, r is nearly constant of ≈ 2.5, while for larger fields ($0.05\ \mathrm{T} < \mu_0 H < \mu_0 H^*$) r approaches a value of ~ 2. These values are slightly larger than the ones we expect from the ratio of moving rows, i.e., 4/2 and 5/3 assuming that the vortex density is the same. The values can, therefore, be explained if we assume that the vortex density in the outer rows that participate at the motion in the high-mobility branch is 20–25% higher than the vortex density of the inner rows. This is a likely scenario because we expect that the bending of the flux lines will produce changes in the lattice constant along and perpendicular to the channel.

IV. CONCLUSIONS

In conclusion, we have investigated flow dynamics of vortices driven through easy flow channels bounded by pinned vortices. We have found that the vortex configurations and their dynamics crucially depend on the field history. When the field increases up to a crossover value H^* (FU case) unusual dynamic properties are observed, such as the presence of a kink in the I-V characteristics. Mode-locking experiments convincingly show that the kink is caused by a force induced vortex slip transition from n moving rows for small driving force to $n+2$ rows for high driving force. The effect is explained by the presence of strong screening currents in the channel edges which produce field focusing and bending of the flux lines around the channels. While the dynamics of the outer vortex rows is determined (via shear interaction) by the pinning centers and the disordered vortex arrangement in the NbN film, the inner rows are subject to a different pinning landscape where the intrinsic pinning of the NbGe is dominant. At higher magnetic fields, where the effect of the screening currents becomes less important, the 1D nature of the vortex flow changes to a conventional 2D flow.

ACKNOWLEDGMENTS

We thank N. Saha for a decoration image of channel device. This work was supported by the "Stiching voor Fundamenteel Onderzoek der Materie" (FOM) and ESF-vortex program.

*Present address: Research and Development Center for Higher Education, Kyushu University, 4-2-1, Ropponmatsu, Chuoh-ku, Fukuoka, Fukuoka 810-0044, Japan. Electronic address: Kokubo@rc.kyushu-u.ac.jp

†Corresponding author. Electronic address: sorop@physics.leidenuniv.nl

‡Present address: School of Physics, University of Edinburgh, Kings Buildings, Mayfield Road, Edinburgh EH9 3JZ, United Kingdom.

[1] A. Pruymboom, P. H. Kes, E. van der Drift, and S. Radelaar, Phys. Rev. Lett. **60**, 1430 (1988); A. Pruymboom, Ph.D. thesis, Leiden University, 1988.

[2] N. Kokubo, R. Besseling, V. M. Vinokur, and P. H. Kes, Phys. Rev. Lett. **88**, 247004 (2002).

[3] A. Gurevich, M. S. Rzchowski, G. Daniels, S. Patnaik, B. M. Hinaus, F. Carillo, F. Tafuri, and D. C. Larbalestier, Phys. Rev. Lett. **88**, 097001 (2002); A. Gurevich, Phys. Rev. B **65**, 214531 (2002).

[4] M. J. Hogg, F. Kahlmann, E. J. Tarte, Z. H. Barber, and J. E. Evetts, Appl. Phys. Lett. **78**, 1433 (2001).

[5] L. Van Look, E. Rosseel, M. J. Van Bael, K. Temst, V. V. Moshchalkov, and Y. Bruynseraede, Phys. Rev. B **60**, R6998 (1999).

[6] G. Karapetrov, J. Fedor, M. Iavarone, D. Rosenmann, and W. K. Kwok, Phys. Rev. Lett. **95**, 167002 (2005).

[7] A. Jukna, I. Barboy, G. Jung, S. S. Banerjee, Y. Myasoedov, V. Plausinaitiene, A. Abrutis, X. Li, D. Wang, and R. Sobolewski, Appl. Phys. Lett. **87**, 192504 (2005).

[8] J. F. Wambaugh, F. Marchesoni, and F. Nori, Phys. Rev. B **67**, 144515 (2003).

[9] R. Besseling, P. H. Kes, T. Dröse, and V. M. Vinokur, New J. Phys. **7**, 71 (2005); R. Besseling, Ph.D. thesis, Leiden University, 2001.

[10] R. Besseling, N. Kokubo, and P. H. Kes, Phys. Rev. Lett. **91**, 177002 (2003); N. Kokubo, R. Besseling, and P. H. Kes, Phys. Rev. B **69**, 064504 (2004).

[11] N. Kokubo, R. Besseling, and P. H. Kes, Physica C **412-414**, 362 (2004).

[12] A. E. Koshelev and V. M. Vinokur, Phys. Rev. Lett. **73**, 3580 (1994).

[13] G. Piacente and F. M. Peeters, Phys. Rev. B **72**, 205208 (2005).

[14] R. Wördenweber, P. H. Kes, and C. C. Tsuei, Phys. Rev. B **33**, 3172 (1986); P. H. Kes and C. C. Tsuei, *ibid.* **28**, 5126 (1983).

[15] The field H_p of the first vortex penetration was estimated using the approach from Vodolazov *et al.* (see Ref. 24), assuming that the film has perfect straight edges and there is no pinning. The vortices first penetrate when the Meissner current at the edge exceeds the Ginzburg-Landau depairing current.

[16] A. Schmid and W. Hauger, J. Low Temp. Phys. **11**, 667 (1973).

[17] A. B. Kolton, D. Dominguez, and N. Grønbech-Jensen, Phys. Rev. Lett. **86**, 4112 (2001); Phys. Rev. B **65**, 184508 (2002).

[18] P. Martinoli, Phys. Rev. B **17**, 1175 (1978).

[19] The values of $V_{1/1}$ are determined at the rf amplitudes at which the first maximum occurs in the width of the ML peak.

[20] A. T. Fiory, Phys. Rev. Lett. **27**, 501 (1971).

[21] N. Kokubo, K. Kadowaki, and K. Takita, Phys. Rev. Lett. **95**, 177005 (2005).

[22] A. I. Larkin and Yu. N. Ovchinnikov, in *Nonequilibrium Superconductivity*, edited by D. Langeberg and A. I. Larkin (North-Holland, Amsterdam, 1986), Chap. 11.

[23] P. Berghuis and P. H. Kes, Phys. Rev. B **47**, 262 (1993).

[24] D. Y. Vodolazov and I. L. Maksimov, Physica C **349**, 125 (2000).